DOI:10.28974/idojaras.2025.3.3

IDŐJÁRÁS

Quarterly Journal of the HungaroMet Hungarian Meteorological Service
Vol. 129, No. 3, July – September, 2025, pp. 279–306

Cold-air pool development and covariance analysis of the measured meteorological parameters in the Mohos sinkhole, Bükk Plateau, Hungary

András Dobos*, **Réka Farkas**, and **Endre Dobos**

Department of Geography and Geoinformatics
University of Miskolc, Miskolc, Hungary

**Corresponding Author e-mail: dobosbandi@hotmail.com*

(Manuscript received in final form August 6, 2024)

Abstract— It is a well-known phenomenon that sinkholes, compared to their environment, have a relatively colder microclimate, due to the topographic conditions (closed depressions). Its geomorphological characteristics favors the development of cold-air pools and can cause significant temperature anomalies. This process has been documented in several papers before, but the detailed buildup and breakup, and especially the environmental covariates that drive these processes, are not well documented yet. This paper aims to summarize a three months period measurement (spring of 2023) in Northern Hungary, on the karst plateau of the Bükk Mountains. This plateau is characterized with a complex karst surface development, having interconnected sinkhole systems. The Mohos sinkhole – the largest sinkhole of the area with several contributing smaller sinkholes – was selected for the measurement campaign. A detailed terrain and remotely sensed database were built to characterize the geomorphology and its contribution to the development of the sinkhole's microclimatic system. A sensor system was developed and adopted to the local conditions using 10 directly measured or derived meteorological parameters (air temperature (200 cm, 40 cm), dew point, solar radiation, relative humidity, wind speed, daily evapotranspiration, vapor pressure deficit., and soil temperature), along with two comparison sites from the edge of the sinkhole and from a representative site of the Bükk Plateau, where no major microclimatic derivation factor was assumed. During this period, the Carpathian Basin was characterized by a significant variability of weather patterns, and was optimal to analyze the behavior of the sinkhole's microclimate system based on the regional weather trends and their atmospheric dynamics. Several temperature inversion events were developed and analyzed to describe the relationships between the cold-air pool development and the external meteorological affects. The events were classified into the commonly accepted categories. The results demonstrated that the time of the lowest recorded temperatures was partly independent from the general temperature regimes. The most important factors are the general geomorphological factors, favorable radiation

conditions, and lack of any external physical disturbance. It was also proved that the soil temperature had the largest correlation with the temperature change (r = 0.95), followed by the dew point (r = 0.92), vapor pressure deficit (r = 0.85), wind speed (r = 0.83) and the relative humidity (r = -0.8). That was also documented, that the near-surface dynamics play an important law in the behaviors of the sinkhole microclimate system, thus the buildup and breakup of the cold-air pool.

Key-words: closed basins, cold air, cold-air pool, microclimate, mountain plateau, radiation, sinkhole, temperature inversion, weather dynamics

1. Introduction

In limestone plateau environments, the process of dissolution creates various karst formations, such as sinkholes without outflow (*Hevesi*, 2002). As a result of their concave geometry, the colder, denser air masses converge towards the deepest points (the bottom of the sinkholes), where they are layered inversely. Sinkholes are characterized by a specific microclimate that is colder than their environment, if the conditions for the development of a cold-air pool are given. The operation of microclimate systems in sinkholes are influenced by the topographic factors, surface/land coverage, and atmospheric conditions. The karst plateau of the Bükk Mountains is rich in well-developed sinkholes, which are located between 650–850 m above sea level (located at lower elevation than most of the sinkholes examined in the international literature). With a normal temperature gradient, this altitude generates a cool mountain climate in the Carpathians that is considered cool in the low-average-altitude Carpathian Basin, although it is warmer than the climate of the broader Carpathian region.

However, due to their special microclimate, the sinkholes of the plateau can be characterized by a significant negative temperature anomaly at a regional level. The largest sinkhole on the Bükk Plateau (Hungary) is the Mohos sinkhole (furthermore: MS), where the Institute of Geography and Geoinformatics of the University of Miskolc began measurements in July 2022. The aim of the research is to quantify the climate trends of the sinkhole's microclimate system during long-term data collection and to provide information through case examples on the effects of various atmospheric events, surface coverage, and microtopographic factors on the temperature inversion inside the Mohos sinkhole. The article summarizes the results of the measurement of the spring, 2023. The analysis of the case examples takes into account the current weather conditions, whereas the measured data provide a complex representation of the processes occurring in the bottom of the sinkhole that affect the different air layers and their temperature.

The topographic conditions and different weather events play a decisive role in the formation, development, and breakup of the near-surface inversion that occurs in sinkholes. The meteorological and topographic conditions affect temperature inversion, and the microclimate generated by sinkholes shapes the

spatial and temporal development of the temperature inversion and influences the quality of the inversion buildup (*Whiteman* and *McKee*, 1982; *Dorninger et al*., 2011; *Dobos and Dobos*, 2023).

In the past, for more than 30 years, many measurements have been made worldwide, with the aim of gathering information about the daily evolution of the cold-air pool (*Aigner*, 1952; *Sauberer and Dirmhirn*, 1954; *Geiger*, 1965; *Whiteman*, 1990 and *Eisenbach et al*., 2003).

Findings concerning the strengthening and inhibiting factors, buildup and breakup periods, and the main characteristics of temperature inversion were elaborated as well. Usually, valleys or basins are the areas where temperature inversions are common. However, there was a methodological problem in the case of the examination of the microclimate in terms of the development of the daily wind pattern in primary form assets, such as larger basins and valleys. The downslope wind can affect the inverse air stratification before the local changes in the inflow and outflow conditions, thus influencing its natural evolution (*Pospichal et al*., 2003; *Steinacker et al*., 2007; *Salavec*, 2012). To have a better understanding, attention was directed towards the local, concave karst formations without outflow, that slope towards one point from all directions, namely the sinkholes (*Steinacker et al*., 2007).

The sinkholes also known as dolines, are well separated from the flow systems of their environments, so a specific microclimate can develop in them. The most characteristic feature of the typical microclimate of the sinkholes is the tendency for temperature inversion, which results in unambiguously low daily minimum temperature (hereafter Tmin) values compared to their surroundings (*Clements et al*., 2003; *Steinacker et al*., 2007).

The microclimate of the sinkholes, the interpretation of the measured temperature curves at different heights above the surface, and the direct and indirect factors affecting them have been partially understood through several periodic and permanent experiments and long-term studies. In fact, the absolute Tmin value in Central Europe was recorded at the limestone plateaus of the Eastern Alps, specifically in the Grünloch sinkhole, where a temperature of -52.6 ℃ was measured in 1932 (*Aigner*, 1952; *Sauberer* and *Dirmhirn*, 1954; *Eisenbach et al*., 2003, *Pospichal et al*., 2003). Another prominent example is the ‘Peter Sinks’ sinkhole in Utah in North America, which, due to its special location and dimensions, is studied extensively by meteorologists’ community (*Clements et al*., 2003; *Steinacker et al*., 2007; *Utah Climate Center*).

Within the climate system of karst mountains, there are microclimate systems, which formed due to the orographic condition and are capable of modifying the effects of solar radiation (shortwave), emission (longwave), and flow conditions (*Whiteman et al*. 2004). The Bükk Plateau sinkholes are typically sinkholes created by dissolution that, thanks to their specific topography, are able

to create unique, separate, tertiary (*Wagner,* 1964) microclimate locations by sinking into the surface of the karst plateau or into the dry valleys (*Keveiné Bárány*, 2011).

In Hungary, research on the microclimate of the Bükk Plateau's sinkholes began during the Austro-Hungarian Monarchy, with the aim of instrument calibration (*Dobos*, 2023). Until 2009, only periodic measurements were carried out on the plateau (*Bacsó* and *Zólyomi*, 1934; *Wagner,* 1954; *Keveiné Bárány,* 2011). Since 2009, a group of amateur meteorologists (by the lead of Róbert Kerékgyártó) have been operating a permanent monitoring network in some sinkholes (e.g., Vörösmeteor sinkhole) and in control points. The meteorological station of the University of Miskolc located in the Mohos sinkhole is the newest member of the Bükk Plateau monitoring system; it gathers data at a gap-filling location (*Dobos et al.,* 2024).

The factor which influences most the developing of cold-air pools are the external meteorological affects (wind and cloud), which can erode the partly built-up temperature inversion (*Dorninger et al*., 2011). Furthermore, the microclimate system of the sinkholes are also influenced by surface coverage, which determines the sky-view factor as well (*Whiteman et al*., 2004; *Zhang,* 2005; *Mackiewicz,* 2012). The less forested, open landscape has higher cumulated sky-view factor, with generally higher surface albedo, compared to the forested ones (*Bacsó* and *Zólyomi*, 1934; *Lehmann,* 1970). Therefore, the vegetation coverage within the system and its direct surroundings is considered the principal factor of the microclimate system. Inside the sinkhole, vegetation adjusts to the decrease in average temperature and to the aspect. The inversed layering of the vegetation is typical. Starting from the bottom of the sinkhole, where cold-tolerant communities are present, within small area a sharp change can be observed, and the vegetation gradually transforms into the regular communities which can be found at the given area, thus moving upwards the inversed vegetation moves towards normalization (*Horvat,* 1952; *Egli,* 1991; *Özkan et al.,* 2010; *Bátori et al.,* 2014a,b).

Snow covering changes the albedo, meaning that its effect on the sinkholes microclimate system is significant. Seasonal snow coverage results in noteworthy difference in the inversions temperature curve and dynamics that develops under similar atmospheric conditions. In addition, snow coverage highly affects the temperature of near-surface soil that is most exposed to atmospheric conditions. The extent of correlation between air and soil temperature decreases with the increase in snow thickness (*Goodrich,* 1982; *Thorn et al.,* 1999; *Beltrami,* 2001; *Sokratov and Barry*, 2001; *Decker et al.,* 2003; *Dobos,* 2024).

2. Materials and methods

2.1. Pilot area description

The investigated area includes the southern third part of Zsidó meadow (Bükk Plateau), the Mohos sinkhole and the contributing area to its microclimatic scope. The MS is the largest sinkhole, of the plateau having an area of 51.097 m². It is located in the Bükk Mountains, which are part of the of North Hungarian Mountains range and can be characterized as the southernmost member of the Northwestern Carpathians (*Kocsis*, 2018). The study area is located in the southwestern part of the platean – located at the southern edge of the northern part of the Bükk. Its elevation exceeds 900 m elevation (*Fig. 1*).

2.2. Data collection methodology

The data measured according to the meteorological standards are intended to ensure the global comparability and interpretability. An automatic meteorological station (iMETOS 3.3 with its default sensor set) was installed at the deepest point of the Mohos sinkhole. The station records the measured meteorological parameters at 2 m above the surface and the soil temperature (hereafter T(s)) at -5 cm. The logging interval is 10 minutes, during which time the instrument continuously collects measurements, so the average, minimum, and maximum values of the 10-minute interval are transmitted to the receiving side. The parameters measured and calculated by the station are the following (based on product portfolio of iMETOS): air temperature (°C, precision: ±0.8 °C), dew point (°C, ±0.3 °C), solar radiation (J/m², calibration against Kipp & Zonen CMP3 under daylight, abs. error max. 5%, typically 3%), vapor pressure deficit ((VPD) kPa, calculated), relative humidity (%; precision 0–80%: +/-2%; precision 80–100%: ±3%), precipitation (mm, resolution: 0.2 mm), wind speed (km/h, threshold: 1.1 m/s), daily evapotranspiration ((ETO) mm, calculated), and soil temperature (°C, ±0.1 °C), complemented with data related to the status of the station. The station transmits the measured data via a mobile network to the FieldClimate website.

The meteorological station iMETOS 3.3 has been placed in the following position in the bottom of the Mohos sinkhole: longitude (WGS1984): 20.463171, latitude (WGS1984): 48.065424, altitude (height of data recording): 825,5 m a.s.l.

The control measuring points (temperature data loggers, installed with a radiation shield in 2 m above the surface) are placed in the following altitude: K1 control point: 888 m, K2 control point: 855 m (see in Section 3.3). Control measurements are taking place in the Mohos sinkhole with the reason to determine the proportion of the air temperature (T) anomaly caused by thermal inversion.

Aside from the permanent monitoring location at the bottom of the MS (at the altitude of 825.5 m, centrum point of cold-air pool developing), there are two control points to provide reference data. Point K2 (855 m) is temporary, it is

located in the eastern outline of the MS (characterized by significant potential of temperature inversion by the model Cold Air Flow (*Schwab,* 2000)). Point K1 (888 m, without potential of temperature inversion by the model Cold Air Flow) is located on the northern side of the Bükk Plateau, at a mountain saddle formation, at Bánkút (*Fig.1*). The elevation difference between points MS and K2 is approximately equal to the difference between points K1 and K2.

In the case of the sinkhole's microclimate, it is also important to know the temperature of the air layers near the surface, so a temperature data logger was installed at 40 cm above the surface onto the meteorological station at the bottom of the sinkhole. The Voltcraft DL-240k data logger is calibrated at the factory; its measurement resolution is ±0.1 °C with ±1 °C accuracy. In order to record possible short-term events, the sensor operated with a 5-minute data recording interval. Such events can take place in the near-surface air flow system of the sinkhole, which are not always detectable at 2 m. The temperature data were recorded and processed on a °C-based scale.

The necessary data for building the digital surface model were collected on site with UAV survey. Georeferenced aerial images in the RGB+Infra range spectrum were taken with DJI Mavic 2 and 3 drones, which flew into the area specified in advance for the authorities. The records were processed with online software called PIX4D Cloud, from which a digital surface model (DSM), orthomosaics, 3D mesh, and point cloud were derived and downloaded.

3. Results

3.1. Delineation of the research area

Fig. 1, shows the digital elevation model (I., DEM) of the Bükk Plateau with the potential areas of cold-air pool within the control points, the digital surface model (II., DSM) and the orthomosaic (III.) image of the sinkhole and its contributing area.

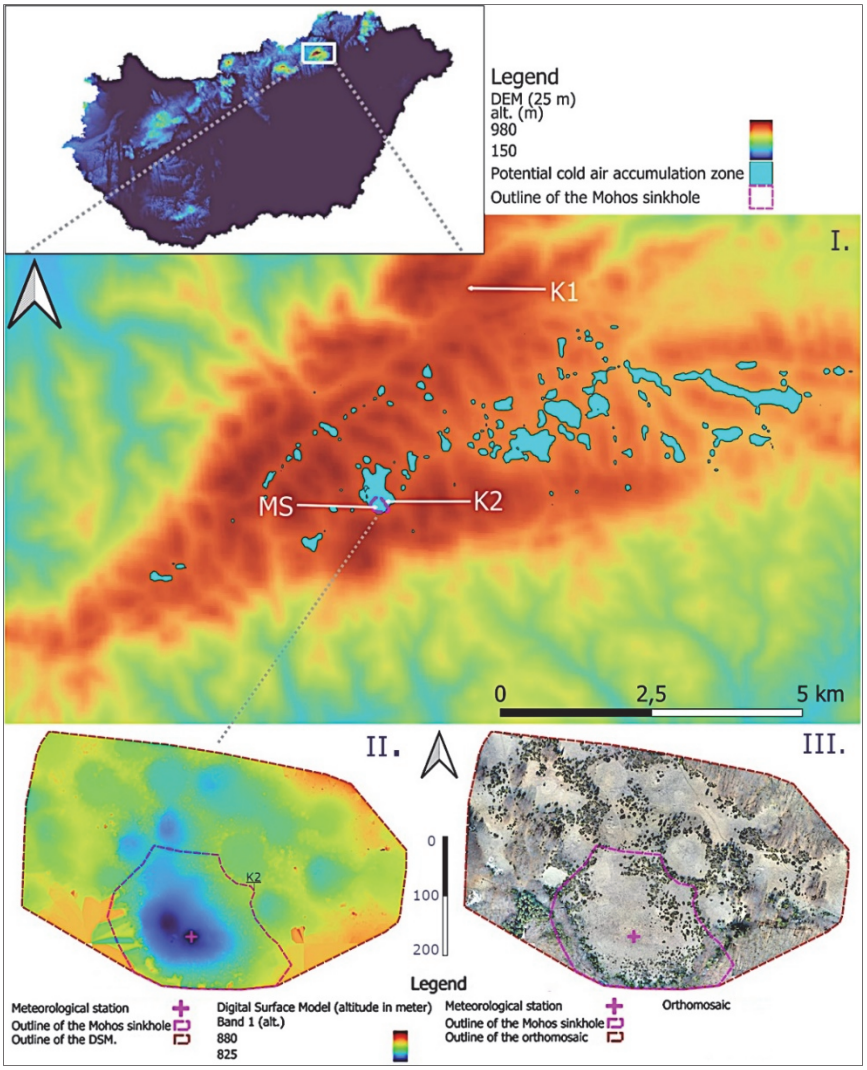

Fig. 1. I.: The location of the control points in the DEM (25 m resolution) of Bükk Plateau and its environment. The blue polygons with a black outline mark the potential areas of the cold air accumulation, calculated by SAGA GIS, tool Cold Air Flow. The Mohos sinkhole meteorological station is marked by MS (centrum area of cold air depositing, place of the meteorological station), the two control points are marked by K1 (area without significant inversion potential) and K2 (outline of the Mohos sinkhole). II.: The high resolution (2.7 cm) digital surface model (DSM) and III.: the orthomosaic of the research area. The broken red line marks the outline of the research area and the dashed pink line marks the outline of the Mohos sinkhole (ridge between the sinkholes). Text K2 in a DSM (left) marks the point of the control measurement (*Dobos*, 2023).

3.2. GIS analysis of the topographic environment of the Mohos sinkhole

The double base and protruding depth of the MS are visible in the southern quarter of *Fig. 1*. Next to it, a number of smaller sinkholes can be seen in the NW and NE directions from the sinkhole. The darker colours of the DSM image represent the double base of the Mohos sinkhole. The protection of the cold-air pools is capacitated by the double bottom of the sinkhole. The most significant elevation decrease begins in the vicinity of the bottom of the sinkhole with the lowest radiation potential within the sinkhole. With the exception of the surrounding steeper slopes around the bottom of the sinkhole, we encounter surfaces with a

much lower slope angle whose confluence point is the bottom itself (moderate blue in *Fig. 1*).

Thus, within the contributing area of the MS, which is most affected by the tertiary microclimate (*Wagner,* 1964; *Keveiné Bárány*, 2011), the less steep, more open-to-the-sky surfaces represent an area with good potential radiation (longwave emission) and high energy loss. The cold air, generated near the surface moves to the direction of the more protected sink bottom and accumulates in an inversely layered manner in the relatively steep twin base, which flattens out again at the bottom (*Fig. 2*).

Accordingly, the sinkhole has a sufficiently high, summarized 'sky-view factor' (index-number referring to the surface exposure to the sky), yet it is able to provide a more protected space for the buildup of the cold-air pool (*Whiteman et al.,* 2004). Due to the geometry of the MS and its surroundings, the microclimate resulting from emitted heat loss provides a favorable environment for the development of relatively low temperature values compared to the surrounding area. The orthomosaic shows that the vegetation also outlines the contours of the dolinas. The vegetation zone inversion, which is typical of larger sinkholes (*Pospichal et al.,* 2003), can also be observed in the Mohos sinkhole (*Figs. 1* and *2*).

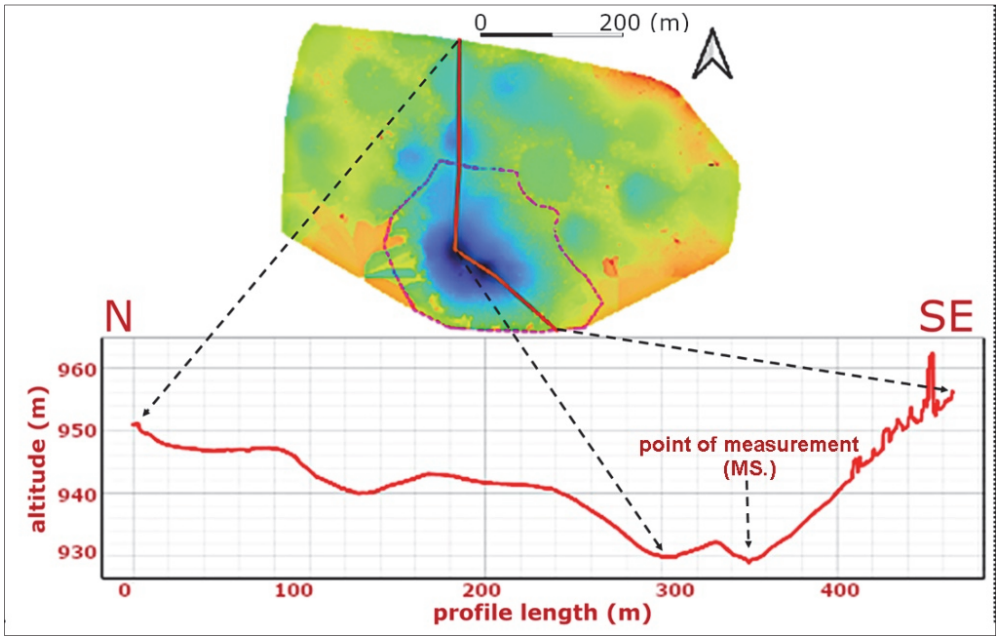

Fig. 2. The elevation (surface) profile (in meter) of the bottom line (from N to SE) of Mohos sinkhole and the environments flow system (marked by a red line across the DSM). The elevation profile was calculated from the DSM's surface, thus it also shows the vegetation on the upper part of the sinkhole's slope (*Dobos*, 2023).

3.3. Control measurements

For comparison, 7 cases were chosen randomly from the periods when thermal inversion was present at the MS. During these 7 cases the average difference of MS and K2 point was 7.4 °C, while the average difference (calculated from the 7 days) of MS compared to the control point K1 was 13.8 °C (*Table 1*). The differences between the MS and K1 ($p=0.0016$) and the MS and K2 ($p=0.04$) were statistically significant. The recorded control values unambiguously confirm the negative temperature anomaly of the Mohos sinkhole in the Zsidó meadow. Moreover, they clearly represent the milder temperature nature compared to the MS, and the definitely present cold temperature anomaly of the Zsidó meadow, compared to the areas not characterized by significant temperature inversion tendencies, but located at a similar elevation (K1).

Table 1. Minimum temperatures (daily Tmin) of the Mohos sinkhole (MS) and control stations and their differences on randomly chosen representative days. The data collection happened in 2 meter above the surface by the same methodology

Altitude	825.5 m	855 m	888 m			
Date of measurements	MS daily Tmin (°C)	K2 daily Tmin (°C)	K1 daily Tmin (°C)	MS dif. compared to K2 (°C)	MS dif. compared to K1 (°C)	Snow cover (cm)
January 9, 2024	-22.31	-15.7	-9.4	-6.61	-12.91	2–4
January 10, 2024	-22.95	-16.3	-8.6	-6.65	-14.35	2–4
January 11, 2024	-21.14	-13.8	-6.1	-7.34	-15.04	2–4
April 13, 2024	-6.26	0.7	9.1	-6.96	-15.36	no
April 21, 2024	-13.7	-6.1	-0.3	-7.6	-13.4	no
April 26, 2024	-12.39	-4.9	-0.7	-7.49	-11.69	no
May 10, 2024	-7.64	1.4	6.3	-9.04	-13.94	no
			average difference: (°C)	-7.38	-13.81	

3.4. Meteorological summary

Information on the regional weather trends of the investigated period is important to interpret the resulted values measured in the MS. The spring of 2023 included alternating, significantly warmer and colder periods compared to the average, and the average temperature rarely adjusted to the long-term average. Overall, the entire

investigated period can be characterised as having temperatures close to average or slightly below the average. Based on the measurement network of the Hungarian Meteorological Service (HungaroMet, 2023a) March brought above-average temperatures (<+1.5 °C) and precipitation in the northeastern region of Hungary. The lowest temperature was -9.2 °C (HungaroMet, 2023a, Zabar, at 4th and 17th of March). April brought below-average (<-2 °C) temperatures and above-average precipitation, while May had a negative temperature anomaly of -1 °C and slightly below-average precipitation. The T-min. recorded by the national official monitoring system in April was -7.8 °C (HungaroMet, 2023b, Kékestető, at 5th of April), while in May, it was -1.9 °C (Hungaromet, 2023a, Zabar, at 9th of May).

3.5. Data processing of the Mohos sinkhole meteorological station for the period March 1 – May 31, 2023

Data from the entire examined period are illustrated in *Fig. 3*. Periods that are colder than the national average do not always cause below-average, 'egregiously' cold temperature values in sinkholes. The development of the cold-air pools and Tmin values that are considered low in the given environment, are the necessary conditions for heat radiation to be present. These conditions are clear sky and wind lull. Periods characterized by nationally and regionally measured negative temperature anomalies are often linked to highly dynamic meteorological events, such as weather fronts. In this case, in addition to the homogenizing wind that prevents inversion, cloudy and rainy weather is also typical. A good example of this is the period of April 1–11, when there was a stable negative temperature anomaly nationally and regionally for a long time, but despite the low dew point, the atmospheric dynamics did not allow the sinkhole's microclimate system to prevail. So, the cold-air pool could only develop for a short time, causing a relatively small daily temperature fluctuation. The period May 15–20 is an example for a similar event (*Fig. 3*).

Apart from the sinkhole's microclimate and its environment's low temperature values, the existence of the radiation conditions is more important than the anomaly towards which the regional weather is moving in the long-term average. As an example, the period of March 1–5 can be mentioned. This period had minimum values below -10 °C each day, and the daily Tmin value dropped below -15 °C four times, which resulted in slightly above-average national and regional anomalies. On March 5, a meteorological front system arrived (HungaroMet, 2023a) and by March 8, the high atmospheric dynamics made the inversion buildup impossible, and the regular daily temperature fluctuation also nearly ceased (*Fig. 4*). The period of March 1–8 (*Fig. 4*) spectacularly illustrates the difference caused by the effect of the microclimate system of the MS between a period characterized by optimal nocturnal radiation and low atmospheric dynamics (March 1–5), and a non-optimal period characterised by strong atmospheric dynamics (March 5–8) (*Fig. 4*). From March 1 to 5 there are 5 cases

of inversion buildups, representing different types. From March 5 to 8 there is a period characterized by a high level of atmospheric dynamics, without inversion build up in the investigated sinkhole.

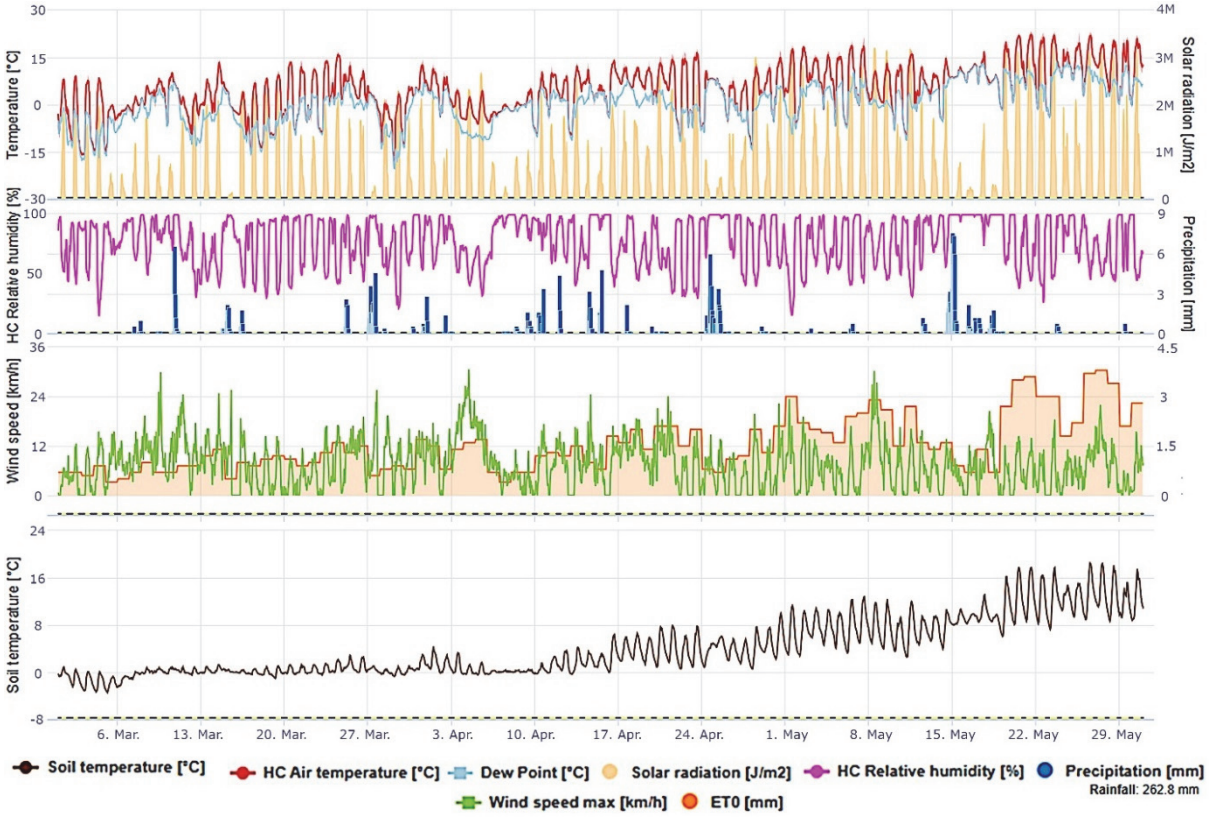

*Fig. 3.*Meteorological parameters measured in 10-minute resolution at the MS station, 2 m above the surface, in the period of marcj 1 – May 31,2023: air temperature (°C), dew point (°C), solar radiation (J/m²), relative humidity (%), precipitation (mm) wind gust (km/h), daily ETO (mm/day), and soil temperature (°C).

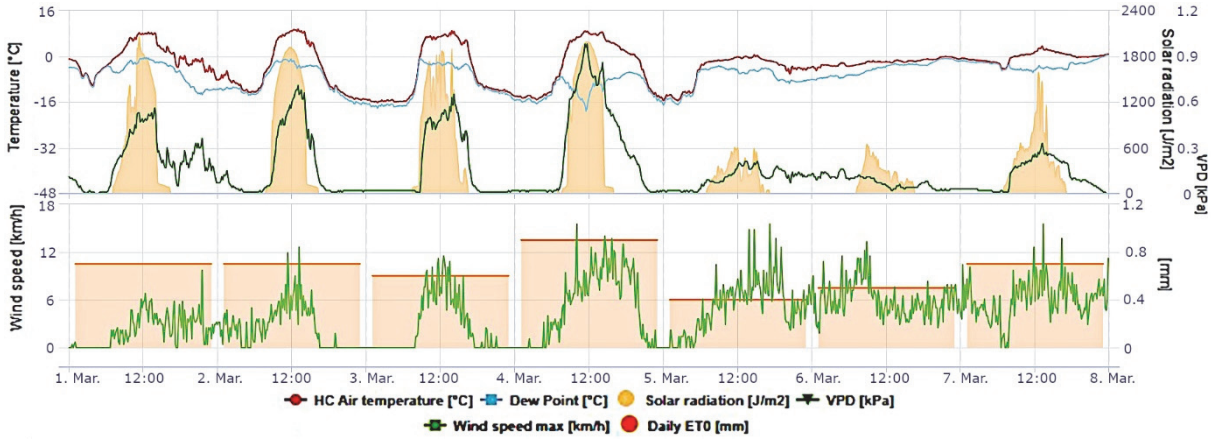

Fig. 4. Meteorological parameters measured in the bottom of the MS, 2 m above the surface, in the period of March 1–8, 2023: air temperature (°C), dew point (°C), solar radiation (J/m²), VPD (kPa), wind gust (km/h), and daily ETO (mm) in hourly resolution.

The period of March 16–24 brought a strong positive temperature anomaly. A negative temperature anomaly was typical for two days, then a strong positive temperature anomaly was observed starting on March 18. However, the temperature inversion was able to develop in the examined area, which meant locally low minimum temperature values, in some cases with values below -10 °C. The period ended on March 24 due to a cold front branch of an incoming weather front system. Following the front, a colder arctic air mass flooded the Carpathian Basin and remained until the March 31 (HungaroMet, 2023a). Minimum values below -10 °C returned to MS. On March 29, the absolute minimum temperature value (-19 °C) of the spring of 2023 was recorded (*Fig. 3*).

To summarize, the most favourable periods for the microclimate to prevail in the MS, which, in local conditions, bring low minimum values and significant daily temperature fluctuations, were March 1–5, March 15t–24, March 27–30, April 9–14, April 20–29, May 1–15, May 19t–23, and May28–31. The value of the relative humidity was determined by the physical characteristics of regional air masses in more dynamic periods from an atmospheric point of view, while in the case of the sinkhole microclimate, it was affected by daily local parameters. In the spring of 2023, 262.4 mm precipitation fell in the MS, distributed evenly. The amount of daily evapotranspiration varied based on the combined effects of the solar radiation, relative humidity, and wind. The lowest values were present at the beginning of the period, in calm weather, with lower solar radiation values. The highest values were measured at the end of the period, with higher solar radiation values and wind. The temperature of the upper layer (-5 cm) of the soil in the bottom of the sinkhole was adapted to the air temperature, including irradiation (shortwave) and radiation (longwave) conditions. At the beginning of the period, with lower solar radiation values, the temperature fluctuation of the typically frozen near-surface soil layer was significantly lower than at the end of the period, despite the similar daily air temperature fluctuations. The reason of this is the increase in the amount and length of daily solar radiation, the own shadow of the sinkhole, and the fact that the heat gain of the thawed soil cover is not hindered by the ice present in the pores of the soil grains. The ground was not covered with snow during the investigated period (*Fig. 3*).

3.6. Typical values of the examined months

The monthly average temperature (*Table 2*) in March 2023, calculated from 10-minute average temperatures, according to the values recorded at 2 m in the MS, was 0.64 °C, while it was 3.5 °C in April, and 9.7 °C in May. The growth of the average temperature was not linear. The highest daily temperature was 16.8 °C in March, 17.8 °C in April, and 23.8 °C in May. The lowest daily temperature was -19.0 °C in March, -13.3 °C in April and -10.7 °C in May. This means that the Tmin value of all three spring months was below -10 °C. The value of the lowest dew point was -21 °C, implying that there was only a 2 °C difference between the

Tmin and the dew point. The relative humidity varied between 99.3% and 11.2%, the average value was 75.4–77.8%; almost the same interval characterized the examined months. The average solar radiation value was 361,720 J/m² in March, 430,911 J/m² in April and 684,024 J/m² in May. The increase in the measured value is not linear, because although the length of the days in the spring period theoretically increases on an equal scale, the absolute incoming solar radiation is greatly modified by the cloud cover and topographical conditions. In the case of the MS, the mountain ridge around has an elevated importance in the reduction of the solar radiation during the winter half year. The highest average daily wind speed was 8.6 km/h, 10.1 km/h, and 10.8 km/h in March, April and May, while the highest absolute wind speed was 29.9 km/h, 30.6 km/h, and 30.2 km/h in March, April, and May. The minimum soil temperature T(s) was -3.6 °C in March, -0.4 °C in April and 2.2 °C in May. The average T(s) in March was exactly 0 °C; it was 2.5 °C in April and 9.8 °C in May. The average value of the near-surface T(s) for all three months is within 1 °C of the air temperature. This leads to the conclusion that the T(s), although it fluctuates in a smaller value range, follows the daily path of the air temperature and changes with its approximate average (*Table 2*).

Table 2. Summary table of measured parameters in the Mohos sinkhole

Mohos sinkhole (2 m)	Air temperature [°C]			Dew Point [°C]		Solar radiation [J/m²]	Relative humidity [%]			Precipitation [mm]	Wind speed max. [km/h]	Soil temperature [°C]		
Date	avg	max	min	avg	min	avg	avg	max	min	sum	max	avg	max	min
March 2023	0.6	16.8	-19.0	-3.9	-21.0	361720	75.4	99.2	11.8	76.6	29.9	0.0	3.3	-3.6
April 2023	3.5	18.0	-13.3	-0.5	-14.7	430911	78.3	99.3	27.1	98.2	30.6	2.5	10.7	-0.4
May 2023	9.7	23.8	-10.7	5.0	-14.5	684024	77.1	99.3	11.2	88.0	30.2	9.8	19.1	2.2

3.7. Comparison of the coldest days by each month

Fig. 5 shows the Tmin curves of March, April, and May in 2023, measured at 2 m. The process of the buildup of the temperature inversion can be characterized as late in the case of March and slightly disturbed in April and May. The daily temperature fluctuation on the coldest day of each month was 23.7 °C in March, 23.9 °C in April, and 28.5 °C in May. The cooling phase of the curves, depicted between 18:00 p.m. and 09:00 a.m. (CET) is steepest in the case of March, while on the coldest days of April and May, the temperature cooled from the initial

values of 6.1 °C and 11 °C to -13.3 °C and -10.7 °C. Their curves intersected around 21:00 and peaked at 5:10 and 4:10, with a difference of 2.6 °C. They exit the chart at 09:00, at 6.5 °C and 11.7 °C.

The running dynamics of the curve of the lowest temperature in March differ significantly from the minimum temperature curves of the following months. At 01:20, the temperature, which had been almost stagnant until then, began to drop intensively. Then, in 40 minutes, it cooled down to 5.9 °C. It 'peaked' -19 °C, at 06:20. The March temperature curve left the chart area at -3.1 °C at 09:00. The time of occurrence and the interval of the warming phase of the three curves illustrate the shortening of the nights in the spring period and the duration of the potential longwave radiation periods. The monthly Tmin shifted by roughly 1 hour during the examined period.

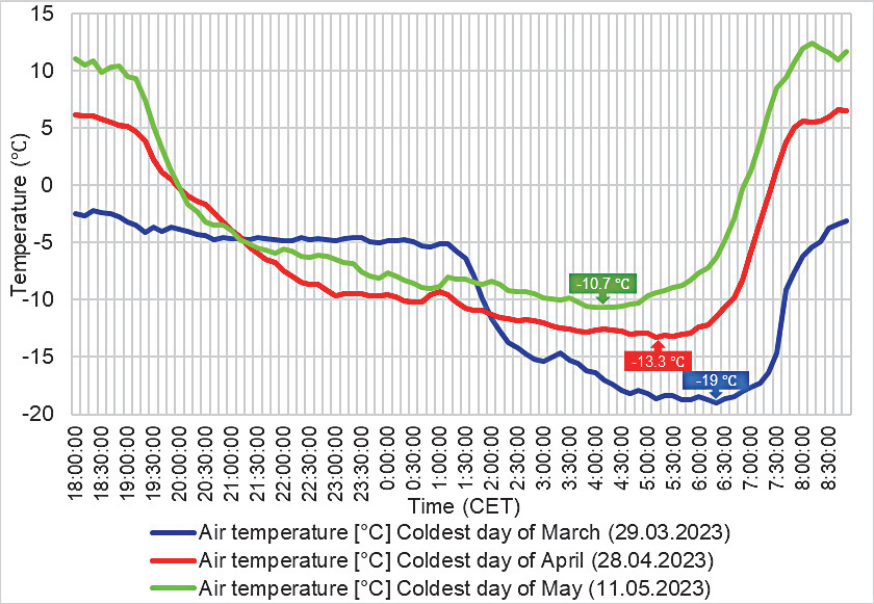

Fig. 5. Tmin curves of the coldest days of each month, recorded in the bottom of the MS, 2 m above the surface in the same time scale from 18:00 p.m. to 8:30 a.m. (CET).

Table 3 contains the daily data for the coldest days of each month in the spring period of 2023. Out of the three examined days, only in the case of March did the daily average temperature fall below 0 °C, and in all other cases, the daily Tmax value stayed above freezing. In no case did the temperature of the air layer located at 2 m reach the dew point. The amount of daily absolute solar radiation tends to increase from 492,750 J/m² to 1,010,200 J/m² as the summer solstice approaches. The minimum value of the daily vapor pressure deficit (VPD) (in kPa) is always 0 kPa during the most significant part of the nocturnal longwave radiation period, and the maximum value varies between 0.2 kPa and 0.5 kPa

towards the end of the period. The daily minimum value of the relative humidity was the most favorable for strong longwave emission in March (18%). This feature is also reflected in the dew point values, as the difference between Tmin and the dew point in March was 2 °C, while other minimum values characterized by a higher relative humidity remained below it. The maximum wind speed of 19.8 km/h recorded on the Tmin day in April was the highest of the three analyzed days. The T(s) only dropped below 0 °C on the Tmin day in March. The station did not register precipitation during neither of these days.

Table 3. Summary table of the coldest days of 2023 of each month by the relevant measured parameters recorded in the bottom of the MS, 2 m above the surface

Mohos sinkhole (2 meters)	Air temperature [°C]			Dew Point [°C]		Solar radiation [J/m²]	VPD [kPa]		Relative humidity [%]			Precipitation [mm]	Wind speed max. [km/h]	Soil temperature [°C]		
Date	avg	max	min	avg	min	avg	avg	min	avg	max	min	sum	max	avg	max	min
March 29, 2023	-6.2	4.7	-19.0	-14.2	-21.0	492750	0.2	0.0	61.4	94.9	18.8	0.0	14.0	0.0	1.1	-0.7
April 28, 2023	1.9	13.2	-13.3	-3.8	-14.7	853825	0.3	0.0	69.9	98.2	37.0	0.0	19.8	3.9	8.1	0.3
May 11, 2023	5.2	17.8	-10.7	-2.2	-11.7	1010200	0.5	0.0	65.5	96.7	28.4	0.0	16.2	7.1	12.4	2.2

3.8. Comparison of the five coldest days

The T-curves show the temperature change of the inversion that can be determined at a height of 2 m above the surface. In the analyzed interval from 16:00 p.m. (through the night) to 8:30 a.m., in all cases, the T-curve of the five coldest days of spring 2023 show the diverse development of the cold-air pool in the MS (*Fig. 6*). Among, the coldest days, three recorded cases fell during the intervals of March 3–5 and the 17 and 29.

The development curve of March 3 (sunrise at 06:14, sunset at 17:25) was undisturbed, apart from one short period disturbed by wind. Good radiation conditions with clear, wind lull weather (*Dorninger et al.,* 2011; *Dobos,* 2023; *Dobos* and *Dobos,* 2023) was prevailed. As a result, the daily Tmin value was -16.2 °C. Within the comparison interval, the starting temperature was 0.6 °C, the

minimum value was -16.2 °C, and the exit value was -0.5 °C, so the absolute temperature fluctuation of the parsed interval resulting in undisturbed development was 16.8 °C.

The curve of March 4 (sunrise at 06:13, sunset at 17:27) shows a slight but constant disturbance; the breakup of the inversion is much earlier than on March 3. Within the comparison interval, the starting temperature was 5.4 °C, the minimum value was -15.2 °C, and the exit value was 3.8 °C, so the absolute temperature fluctuation of the interval resulting in the development of the inversion was 20.6 °C. This temperature inversion occurred despite the slight disruption of the mixing event affecting its development, it is even higher than the previous interval's fluctuation value.

The curve of March 5 (sunrise at 06:11, sunset at 17:28) indicates the later onset of the inversion buildup within the potential longwave emission period (late buildup) (*Dorninger et al.,* 2011; *Dobos,* 2023; *Dobos* and *Dobos,* 2023). The reason of that is that the level of significant disturbance decreased long after the beginning of the potential longwave radiation period. The breakup of the curve occurred the earliest on the March 5 of the five coldest days examined. Within the comparison interval, the starting temperature was 4.6 °C, Tmin was -15.5 °C, and the exit value was -1.4 °C, so the absolute thermal fluctuation of the interval resulting in the buildup was 20.1 °C. The T-curve indicates a significant and permanent disturbance that affects the development of the temperature inversion, but does not eliminate its existence, because the resistivity of cold-air pool against the external affect is co-evolved with the level of the development (*Petkovšek,* 1992; *Rakovec et al.,* 2002).

The temperature curve showing the formation of Tmin on March 17 (sunrise at 05:46, sunset at 17:46) is a typical example of mixing events. Mixing events are invoked by external influences (wind, clouds) that have an intense effect on the potential period that enables the formation of the inversion, and when they cease, the cold-air pool stabilizes again (*De Wekker et al.,* 2006; *Dorninger et al.,* 2011; *Dobos,* 2023; *Dobos* and *Dobos,* 2023).

The initial value of the temperature curve at 16:00 was 1.2 °C; it cooled down to -11 °C by 20:30. Then, the temperature increased to -3.5 °C by 22:30, and until 1:00, it fluctuated in a narrow range depending on the strength of the wind disturbance. After the abatement and termination of the mixing event, the daily Tmin value stood at -15.5 °C at 5:40, after the wind was moderated again. Following that, the temperature started to rise temperately and then steeply, the mixing event intensified again and then, due to the insolation, it left the area of the diagram at 1.9 °C.

The coldest day of the spring period, in addition to the case of the late buildup of the cold-air pool, occurred on March 29 (sunrise at 06:22, sunset at 19:03), with a daily Tmin of -19 °C. The complex case study of the coldest day of the measured period is described in the following chapter.

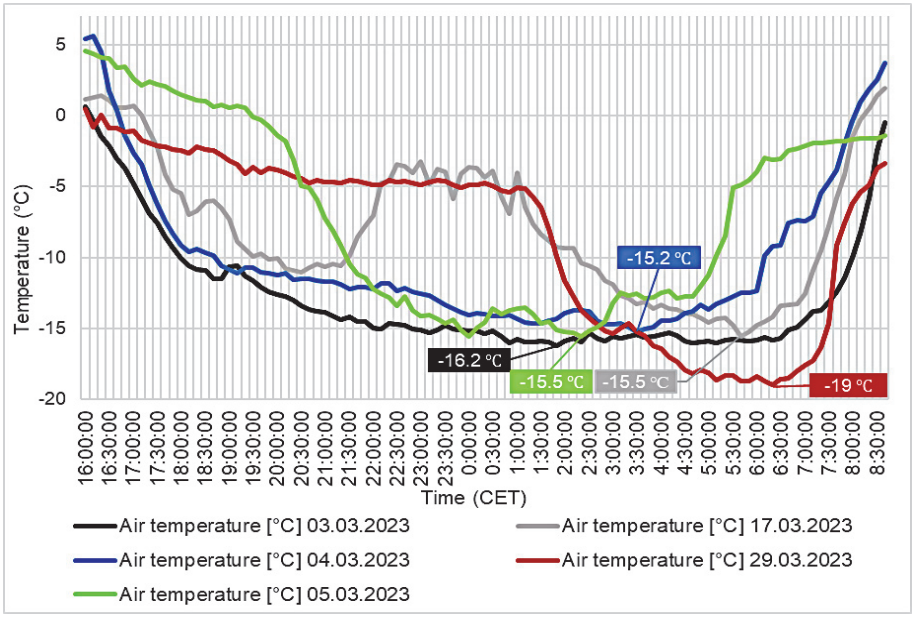

Fig. 6. Air temperature curves of the five coldest days of the period of the spring of 2023, recorded in the bottom of the MS, 2 m above the surface, in a same time scale from 16:00 p.m. to 8:30 a.m. (CET).

4. Case study of the coldest event of the spring of 2023

4.1. Covariance analysis of the measured meteorological parameters in case of late inversion buildup

The recorded data of the absolute Tmin day are listed in *Table 4*. The average temperature on March 29 was -6.2 °C; the temperature extremes were 4.7 °C and -19 °C. The average temperature, measured at 40 cm above the surface was -8.5 °C; the temperature extremes were 3.6 °C and -20.8 °C (at 40 cm only the temperature was recorded).

Table 4. Summary table of the coldest day by all relevant measured parameters

Mohos sinkhole (2 meters)	Air temperature [°C]			Dew Point [°C]		Solar radiation [J/m²]	VPD [kPa]		Relative humidity [%]			Precipitation [mm]	Wind speed max. [km/h]	Soil temperature [°C]		
Date	avg	max	min	avg	min	avg	avg	min	avg	max	min	sum	max	avg	max	min
March 29, 2023	-6.2	4.7	-19.0	-14.2	-21.0	492750	0.2	0.0	61.4	94.9	18.8	0.0	14.0	0.0	1.1	-0.7

Fig. 7 and *Tables 4–6* present the processed database. The examination period presented in the tables covers the period between March 28, 2023 18:00 a.m. and March 29, 2023 09:00 p.m. A variance analysis was performed (*Microsoft Office Professional Plus 2016, Anova: Single Factor* function) to characterize the correlations and statistical covariances of the measured parameters. The results of the ANOVA are summarized in *Table 5*, which quantitatively illustrate the main characteristics of the dataset for the 10-minute averages of the measured values. There were 90 measurements observed for the period. The values of the variation analysis between groups according to the factors are the following: sum of squares (SS) = 478,427.54, degrees of freedom (df) = 5, mean squares = 95,685.51 and F statistic = 2361.1. The P-value is 0 and the F criterion is 2.23. The values within the groups, according to the factors, are SS = 21,640.77, df = 534 and MS = 40.52. Overall, SS = 539 and df = 539. The source of variation shows a significant variance (ANOVA) based on the factor F and P-value where P (0) < 0.05 and F (2361.101) > F crit (2.230896).

Table 5. Table of ANOVA analysis of the database described in Section 4, based on the investigated microclimate event (late buildup of cold-air pool) in the day of the coldest Tmin.

ANOVA Summary

Groups	*Count*	*Sum*	*Average*	*Variance*
Air temperature (°C)	90	-829.16	-9.21289	36.92435
Dew point (°C)	90	-1183.2	-13.1467	19.8996
VPD (kPa)	90	8.45	0.093889	0.005772
Relative humidity (%)	90	6716.72	74.63022	170.2659
Wind speed max. (km/h)	90	389.4	4.326667	15.99951
Soil temperature (°C)	90	-25.4	-0.28222	0.05968

ANOVA

Source of Variation	*SS*	*df*	*MS*	*F*	*P-value*	*F crit*
Between groups	478427.54	5	95685.51	2361.101	0	2.230896
Within groups	21640.777	534	40.5258			
Total	500068.31	539				

4.2. Correlation analysis of the measured variables in case of late inversion buildup

The correlation analysis of the variables of the investigated microclimate event (*Table 6, Fig. 7*) concerns an example of the late buildup (*Dorninger et a*l., 2011) of temperature inversion. The mutual altering of individual variables is more significant within a more dynamic, multifactorial event. Thus, the processing of the microclimate case resulting in the coldest temperature of the spring of 2023 within the selected time scale (the same as the previous) is suitable for the correlation analysis. The solar radiation value is not present in *Table 6*, because of the insolation's non-representative proportion in the examined period, especially in case of late buildup of the cold-air-pool. In the case of correlation analysis, the analysis of an entire period of solar radiation (shortwave) and emission (longwave radiation) would be ideal to use. However, it illustrates the late buildup type of the analyzed temperature inversion case, by presenting the difference between the end of the insolation and the start of the inversion build up (dropping of the T-curves).

Table 6. Correlation analysis of measured variables used in the case described in Section 4.2, based on the investigated microclimate event (late buildup of cold-air pool) in the day of the coldest Tmin.

Correlation	Air Temperature (°C)	Dew point (°C)	VPD (kPa)	Relative humidity (%)	Wind speed max (km/h)	Soil temperature (°C)
Air Temperature (°C)	1					
Dew point (°C)	0.92330214	1				
VPD (kPa)	0.852487159	0.589986648	1			
Relative humidity (%)	-0.796427533	-0.50718294	-0.9898845	1		
Wind speed max (km/h)	0.829947887	0.741720119	0.76561716	-0.717710297	1	
Soil temperature (°C)	0.952531281	0.840751343	0.86311717	-0.813203582	0.776117482	1

According to *Table 6*, the variable that correlates the most with air temperature is the soil temperature ($r = 0.95$), followed by the dew point ($r = 0.92$), VPD ($r = 0.85$), wind speed ($r = 0.82$), and the relative humidity ($r = -7.2$. The correlation with the air temperature is strong for all variables ($r \geq 0.7$). The dew point correlates strongest with the air temperature ($r = 0.92$). It is followed by the soil temperature ($r = 0.84$) and wind speed ($r = 0.74$), which still has a strong correlation. The correlation of the VPD ($r = 0.58$) and relative humidity ($r = -0.51$) with the dew point are moderate. The correlation of the VPD with relative humidity is the strongest ($r = 0.99$), followed by the soil temperature ($r = 0.86$), air temperature ($r = 0.85$), and wind speed ($r = 0.76$). The VPD's covariation with the dew point is medium ($r = 0.59$). Excluding the dew point ($r = -0.51$), the degree of covariation of the relative humidity is strong for all variables, and its range is negative. The correlation of the relative humidity with the VPD is the strongest ($r = 0.99$), since the relative humidity and the momentary difference in the amount of moisture needed to saturate the given air mass have an effect on each other. The VPD is followed by the soil ($r = -0.81$) and air ($r = 0.8$) temperatures and wind speed ($r = 0.72$), which have a strong correlation. The degree of mutual alternation is the smallest among the variables that are strongly correlated with the relative humidity. The correlation of the wind speed with all examined variables is strong without exception. However, a correlation value above 0.8 is only obtained for the air temperature. The covariance values of the other variables are concentrated within a narrow range from $r = 0.71$ to 0.77. The correlation of soil temperature with air temperature is the strongest ($r = 0.95$), however, it should be mentioned that the degree of covariation would be low in the case of snow cover. The degree of covariation of the soil temperature with additional variables is also high in all cases. Overall, it can be said that the studied variables correlate the best with the air temperature (without snow covering, but in case of 2–4 cm snow, $r = 0.57$ and in case of 35 cm snow $r = 0.29$ in -5 cm (*Dobos*, 2024)), but the covariation among almost all variables is strong. The exceptions are the correlations of the dew point with the VPD ($r = 0.58$) and with the relative humidity ($r = 0.51$), which only resulted medium range values. In the period examined in this subsection, there are no weak relationships between the variables. The late buildup type of cold-air pool (temperature inversion) is characterized by the fact that the disturbing events (wind, clouds) that prevent the development disappear late in the potential nocturnal emission period. Thus, causing a delay but creating the conditions for the development of the cold-air pool, which are a clear night sky and calm winds. On the night from 28th to 29th of March, 2023, a typical case of late buildup took place in the Mohos sinkhole (*Fig. 7*).

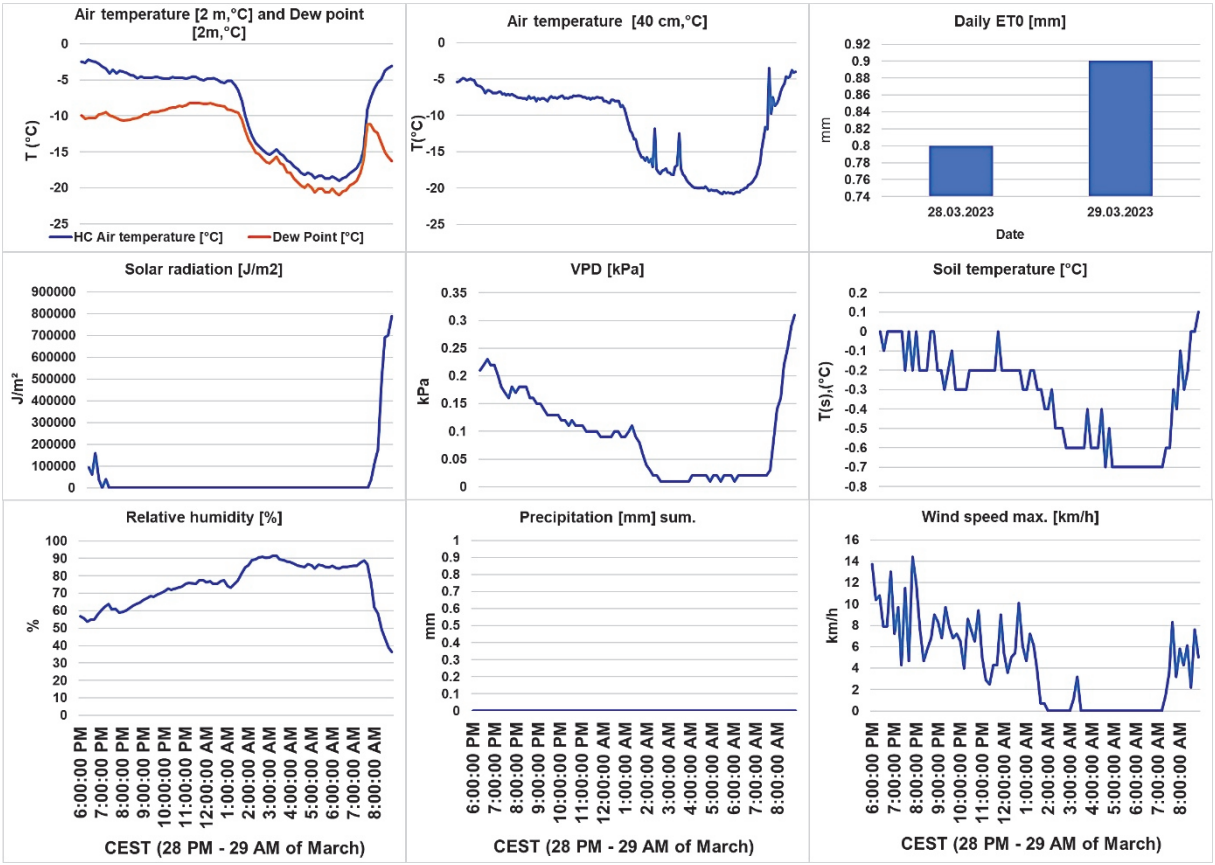

Fig. 7. Typical case of the late buildup of the temperature inversion in the night of March 28–29, 2023 (CEST), in 10 minutes resolution (except the daily evapotranspiration). The presented parameters are the next: air temperatures at 200 cm and 40 cm in °C; dew point at 200 cm in °C; daily evapotranspiration (ETO) at 200 cm, in mm/day (sum.); solar radiation at 200 cm in J/m², vapor pressure deficit (VPD) at 200 cm in kPa; soil temperature at -5 cm under the surface, in °C; relative humidity at 200 cm in %; precipitation at 200 cm in mm (sum) and wind speed at 200 cm in km/h.

The first step of the graphical analysis is the comparison of the air temperature data measured at 200 cm and 40 cm above the surface (from the sinkhole's bottom) in the examined period. The rakes of the T-curves were similar; however, the air layer near the surface were much more unstable and sensitive to external effects than the air layer at 200 cm. The entry value of the temperature curve measured at 40 cm at 18:00 was -5.4 °C, while the one measured at 200 cm was -2.5 °C. The measured difference was almost 3 °C, which remained until the rapid temperature drop starting at 1:00; when the air temperature was -8 °C at 40 cm and -5 °C at 200 cm. At this point, the wind speed began to moderate rapidly, and the dew point and VPD also began to fall as the temperature decreased under conditions that became favorable for the buildup of the cold-air pool. The relative humidity of the rapidly cooling air moved towards saturation and peaked at 91.62% at 3:10. Following that, the air temperature began

to slowly decrease. Between 03:10 and 03:30, a 20-minute windy period broke the dynamics of the undisturbed microclimate system of the sinkhole, causing a slight warming, with a peak value of -14.4 °C at 200 cm at 03:20. The behavior of the air currents detected at 2 m explains the dynamics of the temperature curve at 200 cm, but there was no significant change in the dynamics of the air layer detected near the surface at the same time. In the near-surface temperature (40 cm), between 02:40 and 03:00, a strong warming can be observed from -17.1 °C to -11.8 °C, followed by a cooling up to -17.4 °C. After that, between 03:35 and 04:00, there was also a significant warming and then a cooling from -18.2 °C to -12.5 °C and back to -18.1 °C. The third obvious affect happened near the surface, during the warming period at 07:40, when a maximum wind gust was recorded at 200 cm in the morning and disturbed the near surface air layers. None of the variables measured at 200 cm showed a clear covariation with the change in the air temperature at 40 cm above the surface. From this, it can be concluded that in the late build-up phase, there was a case of lower disturbance in the MS, which stopped the temperature inversion near the surface for short periods (*Dorninger et al.,* 2011; *Dobos,* 2023; *Dobos* and *Dobos,* 2023). The inverse air layering, according to the air density, was immediately restored with the reduction of the stratification of the near-surface air currents, after the cold-air masses close to the surface from the direction of the sinkhole's slopes returned to the bottom of the sinkhole. Following the Tmin occurred at -20.8 °C at 06:20 at 40 cm, the near-surface temperature curve leaves the diagram area at -4 °C. The data of the variables recorded at 200 cm confirm the values indicated by the correlation matrix, implying that the instantaneous covariation of the parameters measured in the given air layer are strong, they respond without exception to external atmospheric effects. It should be emphasized that the fluctuation of the T(s) follows the fluctuation of the near-surface T-curve with a slight delay, especially in the case of outlier disturbances. After the impact of insolation at 7:40, the T and T(s), the dew point and the VPD rise rapidly, the relative humidity starts to decrease accordingly, the microclimate system of the sinkhole is less effective inside the sinkhole, and the turbulent air currents caused by convection are partially eliminated; the temperature inversion forms in the sinkhole, and the temperature inversion disappears or moves to the shaded side of the sinkhole. The temperature inversion persists until the end of the examined period (09:00). The presence of various turbulent airflows is a significant factor in the erosion of the cold-air pool. The eventual outcome of this is proportional to the stability of the cold-air pool and the buoyant force of the turbulent airflow and vertical wind shear (*Petkovšek,* 1992; *Rakovec et al.,* 2002). The threshold for overturning the equilibrium effect is the Richardson's critical value ($R^2 = 0.25$), which can erode the temperature inversion (*Kunze et al.,* 1990; *Glickman,* 2000; *Dorninger et al.,* 2011).

5. Statistical summary of the data measured in the Mohos sinkhole in the spring of 2023

The air temperature-based daily (*Table 7*) and monthly (*Table 8*) summary tables of the spring measurement period of the Mohos sinkhole in 2023 present the quantitative and statistical characteristics of the investigated period in meteorologically relevant categories. The average temperature, calculated on the basis of 10-minute averages for the analyzed period, is 4.6 °C. There is a 16-fold difference between the average temperatures of the coldest and warmest months. The monthly Tmin was always below -10 °C, the absolute minimum value of the measured period was -19 °C at 2 m (-20.8 °C at 40 cm) and Tmax was 23.8 °C. The average of the daily Tmin values in all three months is in the negative range, and for the entire examined period it is -4.4 °C. There is a 11-fold difference between the average daily Tmin values of the coldest (March) and warmest (May) months. The monthly average of Tmax values, which are less affected by the microclimate system as spring progresses, does not show such a large difference. The reason of this is that the main affected parameters of the sinkhole microclimate system are the extremely low daily Tmin values compared to their environment. The monthly temperature fluctuation in all cases exceeds 30 °C; in the case of March, it is 35 °C. The coldest daily average is -6.3 °C. The average temperature of every day in the month of May is positive (*Table 7*).

Table 7. The statistical summary of the measured air temperature values in monthly distribution, recorded in the bottom zone of the MS, 2 m above the surface in °C scale

Mohos sinkhole (2 m) Investigated period	March 2023	April 2023	May 2023	Sum. (all 92 days)
10-minute average °C	0.6	3.6	9.7	4.6
Tmin °C	-19.0	-13.3	-10.7	-19.0
Tmax °C	16.8	18.0	23.8	23.8
Tmin avg. °C	-7.9	-4.7	-0.7	-4.4
Tmax avg. °C	8.8	10.6	18.3	12.6
Monthly absolute temperature fluctuation °C	35.8	31.3	34.5	42.8
Coldest daily average temperature °C	-6.3	-3.6	3.46	-6.3

During the examined 92-day period (*Table 8*), there were 74 frozen days (Tmin ≤ 0 °C) in the MS, which means that 80.4% of the days were below freezing within the period. Only two days in March did not have below-freezing temperatures. The average daily temperature was equal or less than 0 °C 19 times

(20.7% of all days). From the summary, two days (2.2%) remained below the daily Tmax value of 0 °C (Tmax ≤ 0 °C). The station registered 40 daily minimum values below -5 °C (Tmin ≤ -5 °C) in March; this happened 14 times in April and 7 times in May (43.5% of the all 92 days). The station also measured 13 daily minimum values below -10 °C (Tmin ≤ -10 °C) in March; 3 times in April and 1 time in May (18.5% of the all 92 days). The temperature dropped below -15 °C (Tmin ≤ -15 °C) only in March, but this did occur on six days in March (6.5% of the all 92 days). The station did not measure a value of -20 °C or below that at 2 m, it was only registered once, close to the surface (40 cm) (*Table 8*).

Table 8. The statistical summary of the measured air temperature values, in daily resolution, recorded in the bottom zone of the MS, 2 m above the surface in °C scale

Mohos sinkhole (2 m) Investigated period	March 2023	April 2023	May 2023	Sum. (all 92 days)	%
Average daily temperature ≤ 0 °C	14	5	0	19	20.7
Tmax ≤ 0 °C	1	1	0	2	2.2
Tmin ≤ 0 °C	29	27	18	74	80.4
Tmin ≤ -5 °C	19	14	7	40	43.5
Tmin ≤ -10 °C	13	3	1	17	18.5
Tmin ≤ -15 °C	6	0	0	6	6.5
Tmin ≤ -20 °C	0	0	0	0	0.0

6. Conclusions

The data show that in the first third of the measurement period, the expected minimum daily temperature value was close to -10 °C; reaching or exceeding this value was not considered as outlier in the MS (Fig. 3). Daily Tmins below -15 °C were experienced only in March. The mentioned values occurred serially at the very beginning of the period and then in a spot-like manner (*Fig. 4*). There are significant increases in the daily average of the minimum temperature for the examined months; however, in all cases and overall, the average of the daily T-min values remained in the negative temperature range. The temperature fluctuation of the entire examined period was 42.8 °C. The absolute Tmax was 23.8 °C, and Tmin was -19 °C; the T-values were extreme in the negative direction compared to the national averages. The processed case examples are in agreement with the literature; they confirm the results and test methodology of previous studies (*Whiteman et al.,* 2004*; Steinacker et al.,* 2007; *Dorninger et al.,* 2011). The examined temperature inversion presented a build-up, stood, and broke drown manner according to the characteristic features of the identifiable

development type in each case. In some cases, the partial persistence of the temperature inversion during the day was also recorded (*Keveiné*, 2011).

The air temperature correlates strongly with almost all measured parameters, showing the complex nature of cold-air pool development. The highest correlation rate was observed with the soil temperature having an $r = 0.95$. Although the T(s) fluctuates in a smaller value range, it follows the daily path of the air temperature and changes with its approximate average. The correlation with the dew point is $r = 0.92$, the VPD has $r = 0.85$, the wind speed has $r = 0.83$ and the relative humidity has $r = -0.8$. There was no precipitation in the timescale of the case processing, thus the relationship with the other parameters, based on this period are unexaminable. It can be established, that in case of significant microclimatical events, the air temperature has the highest, while dew point and the relative humidity have the lowest correlation with each of the other measured parameters. This result, in agreement with the literature, assumes a low interaction between the inversion build-up and the momentary level of the relative humidity, as long as the air saturation does not exceed the condensation threshold. The reason of that is the fog formation which reduces the value of the longwave surface radiation (*Whiteman et al.,* 2007; *Dorninger et al.,* 2011).

It is important to note, that the degree of covariation of the T(s) with the other measured parameters in the case study was analyzed in conditions without snow covering. The qualitative presence of the snow covering basically affects the degree of correlation of the T(s) with the air temperature (*Goodrich,* 1982; *Thorn et al.,* 1999; *Beltrami,* 2001; *Sokratov* and *Barry,* 2001; *Decker et al.,* 2003).

By the temporary control measurements, the average anomaly levels (between MS and K2, and MS and K1) of the research area are in alignment of the results of what the *Cold Air Flow* model suggested (*Table 1, Fig. 1*). Moreover, based on the measurements, in case of stable inversion build-up, the temperature difference of the daily Tmin values between the bottom of the sinkhole and the K1 and K2 control points do not depend on snow coverage.

Although the near-surface layers of the temperature inversion are exposed to the effect of cold air masses flowing near the surface from the sides of the sinkhole, which often cause momentary disturbances, the regeneration occurs almost immediately after the lower disturbance event. The near-surface air layers are more protected against the external meteorological effects from outside of the sinkhole (*Dorninger et al.,* 2011). By all means the behavior of the near-surface air layers are the most independent regarding the microclimate system of the closed depressions. Further measurements are needed to have a better understanding on them.

Out of the seven selected days with extremely low Tmin values, four (March 17 and 19, April 28, and May 11) dates were below the long-term average temperature, two had average (March 4 and 5), and one had higher than the long-term average temperature in the Hungary (March 3). The days of the official national minimum temperatures recorded by the Hungarian Meteorological

Service never matched with the ones when the Mohos sinkhole minimum records were measured. None of the sinkhole minimums were measured in the nationally recorded colder weather situations. It was concluded, that in case of the sinkhole microclimate, the regional weather anomalies have less impact on the build-up of cold-air pools than the local atmospheric dynamics and their characteristics and expressions. The presence of a topographic microclimate system in the Bükk Plateau's Mohos sinkhole was generally present based on the measured data from the spring of 2023. The data contained the lowest measured temperature value that was detected in the country during the examined period (including the non-official data) (HungaroMet, 2023a).

Acknowledgment: We would like to acknowledge the contribution of the University of Miskolc, Institute of Geography and Geoinformatics for allowing me to use the meteorological station. I also want to thank Róbert Kerékgyártó for sharing with me the data of K1 control point and for the sources of history of science. I also wish to thank the Bükk National Park (BNPI) for kindly granting permission to carry out measurements in the strictly protected area.

References

Aigner, S., 1952: Die Temperaturminima im Gstettnerboden bei Lunz am See, Niederösterreich (The minimum temperatures in the Gstettner basin near Lunz, Lower Austria). *Wetter Leben*, Special Issue *1*, 34–37.

Bacsó, N. and *Zólyomi B*., 1934: Mikroklíma és növényzet a Bükk-fennsíkon. *Időjárás 38*, 177–196. (In Hungarian)

Bátori, Z., Csiky, J., Farkas, T., Vojtkó, E.A., Erdős, L., Kovács, D., Wright, T., Körmöczi, L., and *Vojtkó, A.,* 2014a: The conservation value of karst dolines for vascular plants in woodland habitats of Hungary: refugia and climate change. *Int. J. Speleology 43*(1), 15–26. http://dx.doi.org/10.5038/1827-806X.43.1.2

Bátori, Z., Farkas, T., E Vojtkó, A., Maák, I. E., and *Vojtkó, A.* 2014b: Veszélyeztetett növényfajok Magyarország erdős és gyepes töbreinek lejtői mentén. *Kanitizia 21*(3–4), 53–62. (In Hungarian)

Beltrami, H., 2001: On the relationship between ground temperature histories and meteorological records: a report on the Pomquet station. *Glob. Planet. Change 29*(3–4), 327–348. http://dx.doi.org/10.1016/S0921-8181(01)00098-4

Clements, C. B., Whiteman, C. D. and *Horel, J.D.,* 2003: Cold air pool structure and evolution in a mountain basin: Peter Sinks, Utah. *Appl. Meteor. 42*, 752–768. http://dx.doi.org/10.1175/1520-0450(2003)042%3C0752:CSAEIA%3E2.0.CO;2

De Wekker, S. F. J., and *Whiteman, C. D.,* 2006: On the time scale of nocturnal boundary layer cooling in valleys and basins and over plains. *J. Appl. Meteorol. 45*, 813–820. http://dx.doi.org/10.1175/JAM2378.1

Decker, K. L. M., Wang, D., Waite, C., and *Scherbatskoy, T.*, 2003: Snow removal and ambient air temperature effects on forest soil temperatures in northern Vermont. *Soil Sci. Soc. Amer. J. 67*(4), 1234–1242, https://doi.org/10.2136/sssaj2003.1629

Dobos, A., 2023: A légköri események és a domborzati viszonyok hatása az inverziós légrétegződés kialakulására a Bükk-fennsíki Mohos-töbörben, M.S. thesis, Dept. of Geography and Geoinformatics, University of Miskolc. (In Hungarian) http://midra.uni-miskolc.hu:80/?docId=43397

Dobos, A. and *Dobos, E.,* 2023: Légköri események hatása az inverziós légrétegződésre a Bükk-fennsíki Mohos-töbör eseti példáin keresztül. Bányászati, Kohászati és Földtani Konferencia, 70–75., ISSN 2784-093X. (In Hungarian)

Dobos, A., 2024: A lég- és talajhőmérsékleti viszonyok együttváltozásának vizsgálata a hóborítottság és talajfagy mértékének alapján a Bükk-fennsíki Mohos-töbörben. Bányászati, Kohászati és Földtani Konferencia, 57–63., ISSN 2784-093X.(In Hungarian)

Dobos, A., Kerékgyártó, R., and Dobos, E. (2024). A 2022-2023-as téli szezon összefoglaló elemzése a Bükk-fennsíki Mohos-töbör és Vörösmeteor-töbör mérései alapján. *Légkör 69*, 33–40. (In Hungarian) http://doi.org/10.56474/legkor.2024.1.5

Dorninger, M., Whiteman, C.D., Bica, B., Eisenbach, S., Pospichal, B., and *Steinacker, R.,* 2011: Meteorological events affecting cold-air pools in a small basin. *J. Appl. Meteorol. Climatol 50*, 2223–2234, http://dx.doi.org/10.1175/2011JAMC2681.1

Egli, B.R., 1991: The special flora, ecological and edaphic conditions of dolines in the mountains of Crete. *Botanika Chronika 10*, 325–335.

Eisenbach, S., Pospichal, B., Whiteman, C. D., Steinacker, R., and *Dorninger, M.,* 2003: Classification of cold air pool events in the Gstettneralm, a sinkhole in the Eastern Alps. In Extended Abstracts, Int. Conf. on Alpine Meteorology and MAP-Meeting, Brig, Switzerland. *MeteoSwiss Publ. 66,* 157–160.

FieldClimate.com: https://www.fieldclimate.com/ (03.06.2024)

Geiger, R., 1965: The climate near the ground. Harvard University Press. Massachusetts, Cambridge.

Glickman, T.S. (Ed.)., 2000: Glossary of meteorology. American Meteorological Society.

Goodrich, L.E., 1982: The influence of snow cover on the ground thermal regime. *Canadian Geotech. J. 19*, 421–432. http://dx.doi.org/10.1139/t82-047

Hevesi, A., 2002: Természetföldrajzi Kislexikon. Műszaki Könyvkiadó, Budapest. (In Hungarian)

Horvat, I., 1952: Die Vegetation der Karstdolinen. *Hrvatski geografski glasnik 14*(1), 1–22. (In German)

HungaroMet, 2023a: Napijelentés kiadvány: (03.06.2024.) (In Hungarian) https://www.met.hu/idojaras/aktualis_idojaras/napijelentes/

HungaroMet, 2023b: Elmúlt hónapok időjárása: (03.06.2024.) (In Hungarian) https://www.met.hu/eghajlat/magyarorszag_eghajlata/eghajlati_visszatekinto/elmult_honapok_idojarasa/

Keveiné Bárány, I., 2011: Néhány adat a bükki töbrök mikroklímájához. A Miskolci Egyetem Közleményei, A sorozat, Bányászat, 82. (In Hungarian)

Kocsis K. (főszerk.) 2018. Magyarország Nemzeti Atlasza – Természeti környezet. Budapest, MTA CSFK Földrajztudományi Intézet. (In Hungarian)

Kunze, E., Williams, A. J., and *Briscoe, M. G.,* 1990: Observations of shear and vertical stability from a neutrally buoyant float. *J. Geophys. Res.: Oceans, 95*(C10), 18127–18142. http://dx.doi.org/10.1029/JC095iC10p18127

Lehmann A., 1970: Tarvágás által okozott ökológiai változások az abaligeti karszton. *Pécsi Műszaki Szemle 25*, 15–21. (In Hungarian)

MeteoPont.hu: http://bukk.meteopont.hu/ (03.06.2024.)

Operating Instructions of DL-240k temperature data logger. (03.06.2024.) https://asset.conrad.com/media10/add/160267/c1/-/gl/001931526ML01/hasznalati-utmutato-1931526-homerseklet-adatgyujto-2001372-c-pdf-funkcio-voltcraft-dl-240k.pdf ,

Ozkan, K., Gulsoy, S., Mert, A., Ozturk, M., and *Muys, B*., 2010: Plant distribution-altitude and landform relationships in karstic sinkholes of Mediterranean region of Turkey. *J. Environ. Biol. 31*(1), 51.

Petkovšek, Z., 1992: Turbulent dissipation of cold air lake in a basin. *Meteorol. Atmosph Phys. 47*(2–4), 237–245, http://dx.doi.org/10.1007/BF01025620

PIX4Dcloud: (03.06.2024.) https://cloud.pix4d.com/drive

Pospichal, B., Eisenbach, S., Whiteman, C. D., Steinacker, R., and *Dorninger, M.,* 2003: Observations of the cold air outflow from a basin cold pool through a low pass. International Conference on Alpine Meteorology, Brig, Switzerland.

Product Portfolio of iMETOS 3.3: (2023.05.20) https://efesaro.com/catalogos/Catalogo_Pessl.pdf

Rakovec, J., Merše, J., Jernej, S., and *Paradiž, B.,* 2002: Turbulent dissipation of the cold-air pool in a basin: Comparison of observed and simulated development. *Meteorol. Atmosph Phys 79*(3), 195–213.

SAGA-GIS Tool Library Documentation (v7.8.0), Tool Cold Air Flow: (03.06.2024.) https://saga-gis.sourceforge.io/saga_tool_doc/7.8.0/sim_air_flow_0.html ,

Salavec, P., 2012: Inverzió és légszennyezés, valamint az égetés hatása a levegő minőségére falusi környezetben. *Tolmácsi Kisbíró 11*, 2–3. (In Hungarian)

Sauberer, F. and *Dirmhirn, I.,* 1954: Über die Entstehung der extremen Temperaturminima in der Doline Gstettner-Alm. *Archiv für Meteorologie, Geophysik und Bioklimatologie, Serie B, 5*, 307–326. http://dx.doi.org/10.1007/BF02242757

Schwab, A., 2000: Reliefanalytische Verfahren zur Abschaetzung naechtlicher Kaltluftbewegungen. Freiburger Geographische Hefte, 61.

Sokratov, S.A., and. *Barry, R.G*., 2002: Intraseasonal variation in the thermoinsulation effect of snow cover on soil temperatures and energy balance. *J. Geophys. Res.: Atmosph. 107*.D10: ACL-13, http://dx.doi.org/10.1029/2001JD000489

Steinacker, R., Whiteman, C.D., Dorninger, M. B., Pospichal, S., Eisenbach, A.M., Holzer, P., Weihs, E., Mursch-Radlgruber, A., and Baumann, K., 2007: A sinkhole field experiment in the Eastern Alps. Bull. Amer. Meteorol. Soc. 88, 701–716, http://dx.doi.org/10.1175/BAMS-88-5-701

Thorn, C.E., Schlyter, J.P.L., Darmody, R.G., and *Dixon, J.C.,* 1999: Statistical relationships between daily and monthly air and shallow-ground temperatures in Kärkevagge, Swedish Lapland. *Permafrost and Periglacial Processes, 10*(4), 317–330. http://dx.doi.org/10.1002/(SICI)1099-1530(199910/12)10:4%3C317::AID-PPP329%3E3.0.CO;2-S

Utah Climate Center, https://climate.usu.edu/PeterSinks, 03.06.2024.

Wagner, R., 1964: Lufttemperaturmessungen in einer Doline des Bükk-Gebirges. *Zeitschr. für Angewandte Meteorologie 5*(3–4), 192–199.

Whiteman, C.D. and *McKee, T.B.,* 1982: Breakup of temperature inversions in deep mountain valleys: Part II. Thermodynamic model. *J. Appl. Meteor. 21*, 290–302. http://dx.doi.org/10.1175/1520-0450(1982)021%3C0290:BOTIID%3E2.0.CO;2

Whiteman, C.D., De Wekker, S. F. J., and *Haiden, T.,* 2007: Effect of Dewfall and Frostfall on Nighttime Cooling in a Small, Closed Basin. *J.Appl. Meteorol. Climatol. 46*(1), 3–13 http://dx.doi.org/10.1175/JAM2453.1

Whiteman, C.D., Haiden, T., Pospichal, B., Eisenbach, S., and *Steinacker, R.,* 2004: Minimum temperatures, diurnal temperature ranges, and temperature inversions in limestone sinkholes of different sizes and shapes. *J.Appl. Meteorol. Climatol. 43*(8), 1224–1236, http://dx.doi.org/10.1175/1520-0450(2004)043%3C1224:MTDTRA%3E2.0.CO;2

Whiteman, C.D., 1990: Observations of thermally developed wind systems in mountainous terrain. In: (Ed. *Blumen, W.*) Atmospheric Processes over Complex Terrain, Meteorological Monographs 23 No. 45, American Meteorological Society, Boston, Massachusets, 5–42, http://dx.doi.org/10.1007/978-1-935704-25-6_2

Zhang, T., 2005: Influence of the seasonal snow cover on the ground thermal regime: An overview. *Rev. Geophys. 43*(4), http://dx.doi.org/10.1029/2004RG000157